Enhancing magnetic signals in unexploded ordnances (UXO) detection based on edge-preserved stable downward continuation method

M. Abedi[1*], K. Mosazadeh[2], H. Dehghani[2], A. MadanchiZare[2]

1. School of Mining Engineering, College of Engineering, University of Tehran, Iran
2. Malek Ashtar University of Technology, Tehran, Iran

Abstract

This paper describes an efficient edge-preserved regularization algorithm for downward continuation of magnetic data in detecting unexploded ordnance (UXO). The magnetic anomalies arising from multi-source UXO can overlap at a height over the ground surface while causative sources may not be readily separated due to low level of signal-to-noise ratio of the observed data. To effectively work the magnetic method in the cleanup stage of contaminated area with UXO, the magnetic anomalies of UXO sources should be enhanced in order to separate the locations of different sources. The stable downward continuation of magnetic data can increase the signal-to-noise ratio, which subsequently causes the separation of UXO sources by enhancing the signals. In this study the researchers formulated the downward continuation as a linear ill-posed deconvolution problem. To obtain a reasonable downward continued field, the proposed filter is stabilized in a Fourier domain to regularize the downward solution using the edge-preserved (or total-variation) algorithm. The L-curve method was used to choose the optimum value of the regularization parameter, which is a trade-off between the misfit and the solution norms in the cost function of optimization problem. A synthetic magnetic field was constructed from isolated multi-source UXO anomalies, the results of which show that the data can be stably downward continued to the ground surface. Likewise, a field data set was provided to demonstrate the capability of the applied method in UXO detection. The results of the synthetic and real case study revealed that the observed magnetic anomalies at a specific height of survey over the ground surface have low amplitude, indeed, the causative UXO sources may not be readily distinguished in detection process, especially anomalies from small UXOs. It was shown that the continued data can enhance the locations of UXOs while small ones are not distinguishable in the primary data.

Keywords: *Unexploded Ordnance, Fourier Transform, Inverse Problem, Edge-preserved Algorithm.*

1. Introduction

Shallow geophysical imaging methods are increasingly implemented in anomaly mapping of buried objects on both land and underwater. Geophysical explorations are vastly superior to the traditional surveys as they minimize drastically time, danger and cost factors [1-2]. One of the main buried objects the investigation of which is

underway to develop appropriate geophysical approaches is the unexploded ordnance (UXO).

The aim of UXO cleanup over large contaminated territories is a sophisticated process at all military area. In many cases, the prospected UXO is routinely detected by sensor sweeps (metal detectors) or geophysical surveys, relative to the background of the region of interest (geologic

background and cultural clutter). Geophysical anomalies of UXO bodies result from the contrast in physical properties related to the host medium materials. Localized geological features and other buried cultural objects (comprising of noise objects in UXO detection such as ordnance scrap, cans, wire, etc.) also yield physical property contrast and subsequently cause undesirable geophysical anomalies. Since in many geological conditions, the physical property contrasts between UXO and host medium are large, UXO detection is a straightforward process. The major problem in geophysical-based UXO detection is the existence of false alarms produced by noise objects, which needs the discrimination algorithms in order to distinguish between varieties of anomaly sources. However, there is no general capability to effectively discriminate UXO geophysical anomalies from false alarm anomalies. It has been noted that for carefully executed geophysical surveys, the probability of UXO detection on documented test sites can exceed 90%.. However, the false alarm rate of non-UXO targets excavated against each detected UXO remains quite high. Without discrimination capability between different causative sources, large numbers of false alarm anomalies must be considered as potential UXO sources, with approximately 75% of the cleanup cost spent on project [3-4].

The widespread geophysical methods for UXO detection are total field magnetometers (TFM) and time domain electromagnetic induction (TDEM) [5-11]. The application of these methods by experienced geophysical practitioners during demonstrations at controlled UXO test sites achieves probabilities of detection of UXO in excess of 90% (e.g. [12]). Other geophysical methods which are worth less in UXO detection consist of ground penetrating radar (GPR), frequency domain electromagnetic induction (FDEM) systems, multi-gate TDEM systems, multi-component TDEM systems, multi-component (vector) magnetometers, magnetic gradiometers, gravimetry, and their airborne systems [4] and [13-26]. The TFM and TDEM surveys from a helicopter platform at 1-2 m sensor elevation have shown promise for covering large area under UXO detection. Multi-gate (25–30 time gates), multi-component TDEM systems and multi-frequency FDEM systems have also valuable potential for UXO detection [27-30].

Magnetic data due to multi-source anomalies may overlap at a given height above the ground surface, especially in the unexploded ordnance (UXO) detection. Therefore, a stable downward continuation method as an unstable filter is needed to separate anomalies of multiple UXO targets in order to enhance those locations by increasing the signal-to-noise ratio. The downward-continued signal is sharper and consequently causes better resolution of multi-source anomalies. The main problem associated with UXO detection is the presence of noise. Since applying this filter is an inverse problem in the Fourier domain, the amplification of high frequency data corrupted by noise is so intense during downward continuation of magnetic data that it quickly masks the information of original data, i.e. suppressing lower frequency data. Low-pass filtering removes the high frequency noises but blurs the information signal and subsequently defeats the enhancement of multi-source anomalies [31-34]. Various methods have been proposed to deal with such filter, in all of which increasing the resolution of downward continued data is the main purpose [11], [32] and [35-43]. The stable downward continuation of UXO anomalies in magnetic prospect has been successfully applied by Li et al. 2013 [11], in which incorporating the expected power spectrum of UXO anomalies preserved the spectral properties and subdued the amplification of high-frequency noise.

In this study, the edge-preserved regularization method which has been previously applied to airborne geophysics in potential exploration by Abedi et al. 2013 [44] is used to enhance the signal-to-noise ratio of the observed magnetic data in UXO detection by stably downward continuation of the data. In what follows, the utility and the applicability of the method are examined for both synthetic and field data in magnetic exploration. The results for both the synthetic and real data show that getting closer to the ground surface by downward continuation causes the enhancement of weak anomalies which are not detectable at a conducted height over the desired area. This filter also separates the locations of multi-source UXO anomalies by enhancing those locations while they overlap at primary height. Here, the previously developed algorithm by Abedi et al. 2013 in airborne potential exploration also confirms its applicability in UXO detection.

2. Methodology

Downward continuation (i.e. harmonic extension of potential field) calculates the magnetic field that is closer to the sources of anomalies. Magnetic data at two observation heights are related by convolution of the upward continuation operation with the downward data using Poisson's integral for the half-space as [45]:

$$T_{Z_2}(x,y,\Delta z) = \frac{1}{2\Pi} \int_{-\infty}^{\infty}\int_{-\infty}^{\infty} \frac{T_{Z_1}(X,Y)\Delta z}{[(X-x)^2+(Y-y)^2+\Delta z^2]^{3/2}} dXdY \;,\; \Delta z = z_2 - z_1 \geq 0 \tag{1}$$

where $T_{z_1}(X,Y)$ and $T_{z_2}(x,y,\Delta z)$ are magnetic data at two different heights separated by a vertical distance Δz. Applying two-dimensional Fourier transform to Eq. (1) yields a simpler form in frequency domain as:

$$\tilde{T}_{z_2}(K_x,K_y,\Delta z) = e^{-\Delta z K}\, \tilde{T}_{z_1}(K_x,K_y) \tag{2}$$

where $\tilde{T}_z$ denotes the Fourier transform of T_z, (K_x,K_y) are wave numbers in x- and y-directions, $K = \sqrt{K_x^2 + K_y^2}$ is the radial wave number, and $e^{-\Delta z K}$ is the upward continuation operator. If we consider the Fourier transform of the observed magnetic anomaly at height z_2, i.e., $\tilde{T}_{z_2}(K_x,K_y,\Delta z)$, as the data, and the upward continuation operator $e^{-\Delta z K}$ as a forward operator, Eq. (2) is a linear inverse problem to be solved for a regularized solution of downward continuation problem. The downward continued solution is numerically unstable because of the ill-conditioning nature of the upward operator and the presence of high-frequency noise in the data. We can stabilize the solution of the problem using an alternative regularized operator. In matrix notation, considering that there are N observations of potential data, Eq. (2) can be written in the space and frequency domain as:

$$[d_{up}]_{N\times1} = H_{N\times N}\cdot[d_{down}]_{N\times1} \xleftarrow[F-1]{F}$$
$$[\tilde{d}_{up}(K_x,K_y)]_{N\times1} = G_{N\times N}\cdot[\tilde{d}_{down}(K_x,K_y)]_{N\times1} \tag{3}$$

where F indicates the 2D Fourier transform, d_{up} and d_{down} arethe Fourier transforms of the observed magnetic data and the downward solution, respectively. The matrix H is the upward continuation operator and the forward operator G is a diagonal matrix in which it contains the values of $e^{-\Delta z K}$.

We suppose that the data are contaminated with white Gaussian noise of zero mean and finite variance σ^2. In order to be able to compute an appropriate solution of downward continuation in Eq. (3), the linear relation of this equation can be replaced by a less ill-conditioned nearby relation. Indeed, the unknown downward continuation vector can be estimated by optimizing a Tikhonov cost function as [46]:

$$d_{down} = \arg(\min_{d_{down}}\{|| d_{up} - H\, d_{down} ||_2^2 +$$
$$\lambda \sum_i \varphi_{d_{down}}([L.d_{down}]_i)\}) \tag{4}$$

where $\lambda > 0$ is a regularization parameter and L indicates the $N\times N$ matrix of regularization operator. Here, the matrix L is chosen as the derivative of magnetic field in z direction. The rth vertical derivative of magnetic field data in the Fourier domain is given by:

$$F\left[\frac{d^r T}{dz^r}\right] = |K|^r F[T] \tag{5}$$

where T is the magnetic data and K is the radial wave number. Therefore, the operator $\tilde{L}$ in the Fourier domain corresponds to $|K|^r$ [45]. Edge-preserving regularization has been developed specifically to stabilize the solution, without eliminating sharp variation of model parameters (i.e., the solution). For edge-preserving methods $\tilde{L} = K$ is the first vertical derivative operator, and $\varphi_{d_{down}}(x)$ can be any potential function satisfying some properties determined by Charbonnier et al. 1997 [47]. Here, we use $\varphi_{d_{down}}(x) = \sqrt{x^2 + \varepsilon}$, where ε is a small positive number that makes $\varphi_{d_{down}}(x)$ differentiable. Substituting $\varphi_{d_{down}}(x) = \sqrt{x^2 + \varepsilon}$ in Eq. (4) leads to an approximation of total-variation (TV) regularization which has been extensively used in many image problems [46] and [48-49]. The minimum of the right-hand side of Eq.

(4) can be calculated using the following iterative procedure [47]:

$$\begin{cases} d_{down}^{m+1} = (H^T H + \lambda L^T A^{m+1} L)^{-1} H^T d_{up} \\ \\ A^{m+1} = 0.5 \underset{i=1,\dots,N}{\text{dig}} \left(\dfrac{1}{\sqrt{[L.d_{down}^m]_i^2 + \varepsilon}} \right) \end{cases} \quad (6)$$

where A is a diagonal weighting matrix. It applies the smoothing on the solution adaptively (i.e., steep gradients are penalized less in the Tikhonov gradient method). Starting at initial point d_{down}^0, the solution is iterated until the relative norm $\|d_{down}^{m+1} - d_{down}^m\|_2^2 / \|d_{down}^m\|_2^2$ is less than a given tolerance [44] and [50]. The regularization parameter λ should represent a compromise between the misfit data ($\|d_{up} - H.d_{down}\|_2^2$) and the norm of the solution ($\sum_i \varphi_{d_{down}}([L.d_{down}]_i)$). Here, the L-curve method is applied to acquire the optimum value of the regularization parameter [51-52]. The curve of optimal values of the norm of the solution versus the misfit data often takes on a characteristic L shape. This happens because the norm of the solution is a strictly decreasing function of λ while the misfit data is a strictly increasing function. The sharpness of the "corner" varies from problem to problem, but it is frequently well-defined. For this reason, the curve is called an L-curve [46]. The value of λ that gives the solution closest to the corner of the L-curve is selected as the optimum one.

3. Synthetic data modeling

A set of synthetic prolate spheroid bodies to simulate UXO sources has been assumed to evaluate the capability of the regularized stable downward continuation approach. Table 1 presents the parameters of 16 ordnance items which have been assumed to simulate the UXOs with a simple shape body, i.e. the prolate spheroid. Varieties of causative sources by changing the azimuth and the plunge of the prolate spheroid are generated to construct a real case study. The location and distribution of assumed bodies have been indicated in Figure 1 in 2D and 3D plots. We have attempted to model ordnance items with similar dimensions of the synthetic prolate spheroid in Table 1. The magnetic responses are presented in Figure 2 at height of 2 m to the ground surface, while random noise with a standard deviation of 5% of the data amplitude has been added to be used in the inversion procedure by the edge-preserved stable downward continuation method. The locations of causative UXO sources have been superimposed on Figure 2 with asterisk symbol.

Table 1. Synthetic parameter sets for ordnance item models shown in Figure 1.

|	Ordnance item	Length (m)	Diameter (m)	Volume (m^3)	Sus. (SI)	X Cor. (m)	Y Cor. (m)	Depth (m)	Azimuth	Plunge
1	40mm Grenade	0.0775	0.0425	0.000073	260	12	17	0.06	150	0
2	Hand Grenade	0.1110	0.0630	0.000231	260	14	12	0.09	30	125
3	57mm Projectile	0.1640	0.0600	0.000309	260	9	15	0.15	90	90
4	60mm Mortar	0.2160	0.0600	0.000407	260	6	3	0.2	15	35
5	81mm Projectile	0.4260	0.0780	0.001357	260	11	2	0.3	50	65
6	105mm Projectile	0.4800	0.1050	0.002771	260	9	18	0.35	35	175
7	155mm Projectile	0.7000	0.1550	0.008806	260	16	10	0.45	45	135
8	175mm Projectile	0.8700	0.1750	0.013951	260	5	13	0.55	55	25
9	8in Projectile	0.8600	0.2030	0.018556	260	9	6	0.5	100	45
10	12in Projectile	1.2100	0.3040	0.058551	260	13	7	0.8	65	70
11	14in Projectile	1.4800	0.3560	0.098211	260	5	9	0.9	20	85
12	16in Projectile	1.6900	0.4060	0.145860	260	4	5	1.1	90	55
13	500lb Bomb	1.5900	0.2660	0.058906	260	14	15	1	80	40
14	750lb Bomb	1.2500	0.4060	0.107885	260	15	3	0.85	60	10
15	1,000lb Bomb	1.8400	0.3390	0.110717	260	4	16	1.2	70	90
16	2,000lb Bomb	2.5000	0.4570	0.273383	260	10	10	1.5	0	0
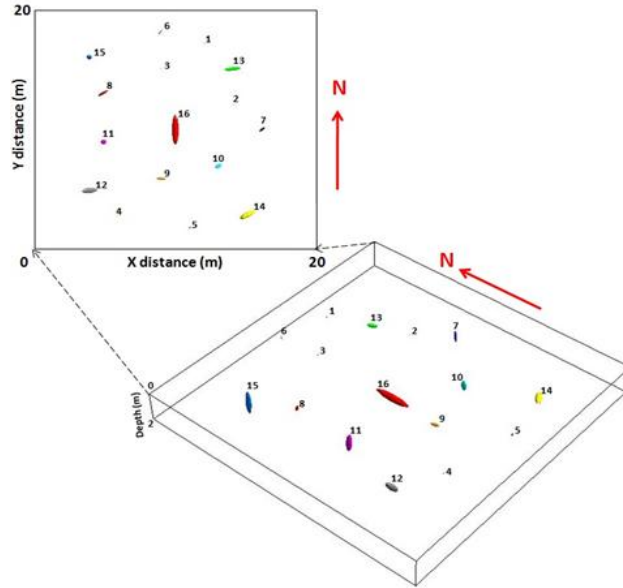
**Figure 1. 2D and 3D plots of the synthetic UXO bodies in magnetic exploration**
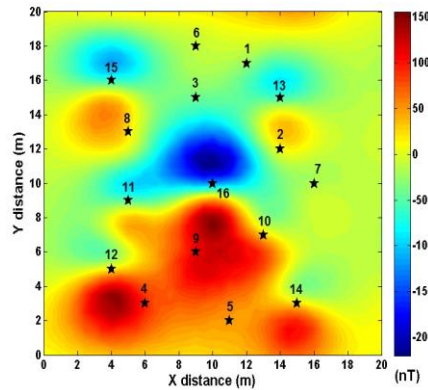
Figure 2. Observed magnetic anomaly over the synthetic models shown in Figure1 at height of 2 m. Random noise with a standard deviation of 5% of the data amplitude has been added.

UXO is generally made of steel and typical susceptibility values of which range from several hundreds to over a thousand in international system of units (SI unit) [8] and [53-54]. Here, we have assumed a fixed value of susceptibility equaling 260 in SI unit for all models (Table 1). Moreover, the inducing magnetic field is 46,000 nT with an inclination of $50°$ and declination of $3°$. The remanence inclination and declination are also $60°$ and $10°$, respectively. The demagnetization effect has been computed as well. We have assumed a constant background susceptibility value equal to 0.001 in SI unit. The sample distance of the synthetic surveys is 0.5 m. Therefore, the observed magnetic data points are 1681.

The edge-preserved stable downward continuation method (or total-variation) is applied at four different height levels, i.e. 1.5, 1, 0.5 and 0 m. Considering the optimum values of the regularization parameter, the proposed method is applied to map the downward continued data of the observed magnetic data at height 2 m. Figure 3 shows the results. The left column shows theoretical magnetic anomaly at height of 1.5, 1, 0.5 and 0 m, respectively. The right column shows continued anomaly from 2 m shown in Figure 2 to four different levels, i.e. 1.5, 1, 0.5 and 0 m. It is obvious that the magnetic anomaly of the synthetic UXO sources in Figure 2 has an overlap and getting closer to the ground surface in the downward continuation yields better resolution of magnetic data and increases the signal-to-noise ratio. Indeed, it causes separation of magnetic anomalies of the synthetic bodies and enhances the locations of the causative

UXO sources. Therefore, using the stable downward continuation method produces the enhanced maps of magnetic anomalies in which the locations of probable UXO sources can be manifested. As a consequence, the continued data reveal further numbers of UXO sources when getting closer to the ground surface. It is the result of the amplification of magnetic anomalies arising from small UXO sources in the continued data while a group of such sources near each other can have an overlapped magnetic anomaly at the primary height, i.e. showing fewer sources.
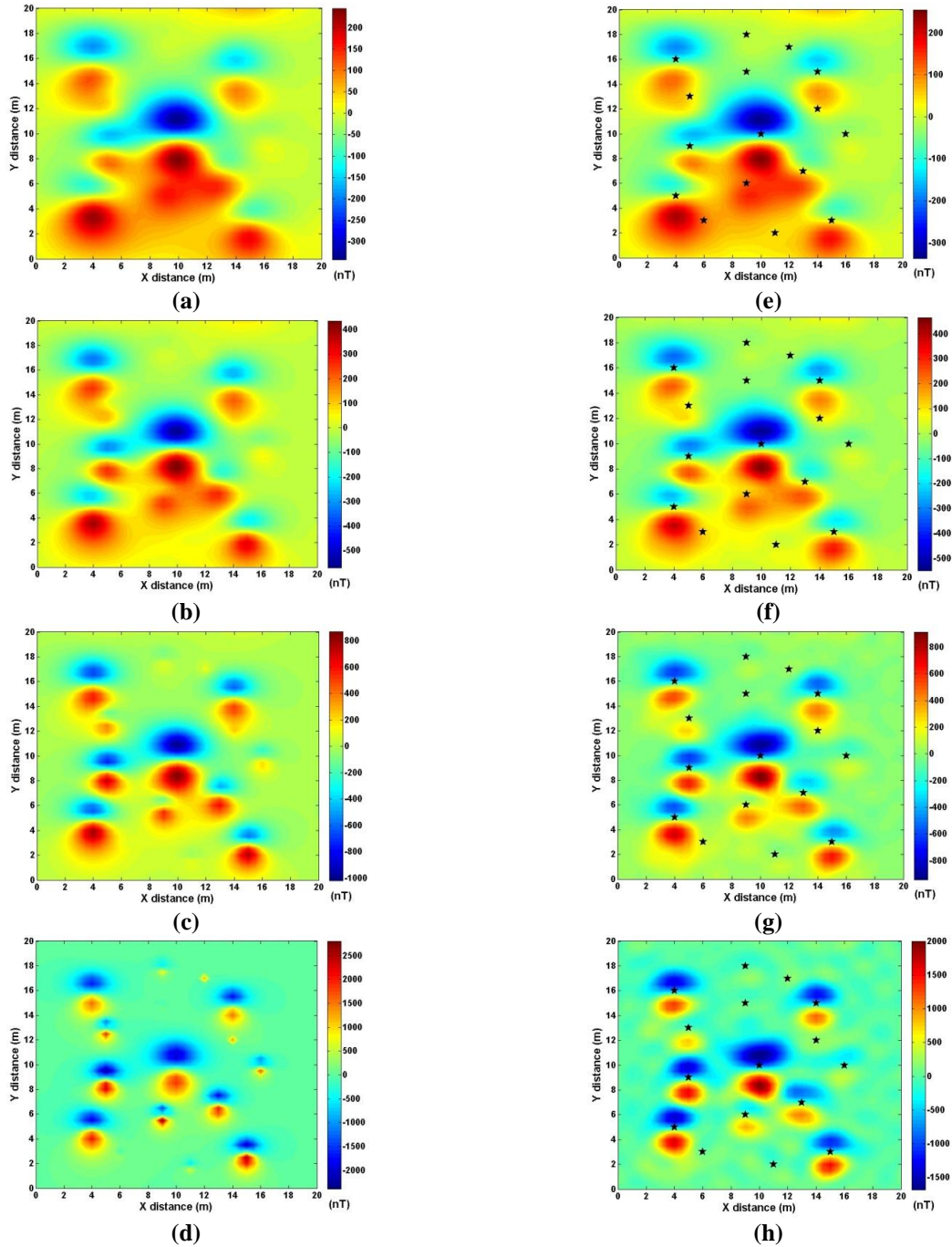

Figure 3. Synthetic example illustrating the effectiveness of the stable downward continuation applied to UXOs' magnetic anomalies. Left panel shows theoretical anomaly at height of, (a) 1.5 m, (b) 1 m, (c) 0.5 m, (d) 0 m. Right panel shows continued anomaly from 2 m shown in Figure 2 to four different levels: (e) 1.5 m, (f) 1 m, (g) 0.5 m, (h) 0 m.

The optimum value of the regularization parameter has been determined by the L-curve method while the solution closest to the corner of the L-curve corresponds approximately to the optimum one. Here, the mean-squared-error score (MSE) of the downward solution and the theoretical data is used to compare the optimum value of the regularization problem with the one obtained by the L-curve method. The left column of Figure 4 shows the normalized MSE score versus λ at which the optimum value of λ minimizes the MSE score for the downward continued solution at heights of 1.5, 1, 0.5 and 0 m, respectively. The right column also shows the L-curve plots of the downward continued solutions at heights of 1.5, 1, 0.5 and 0 m, respectively. The optimum value of the regularization parameter acquired from the MSE score has been superimposed on the L-curve plot with red asterisk, all of which correspond to the corner of the L-curve plot. It proves that the selected regularization parameter using the L-curve method is in well agreement with the optimum one in the MSE score. Therefore, the L-curve method appropriately chooses the optimum value of the regularization parameter in the stable downward solution.
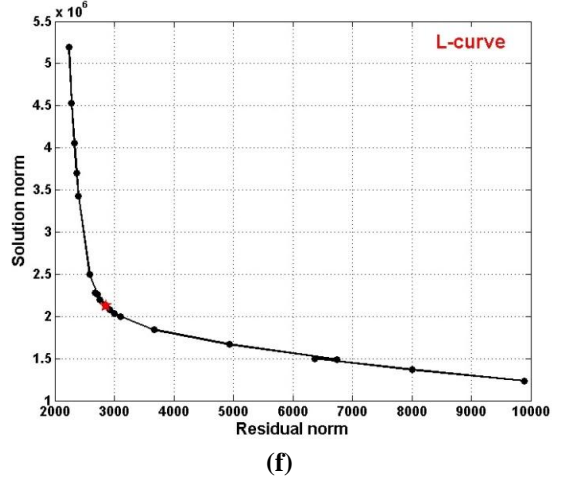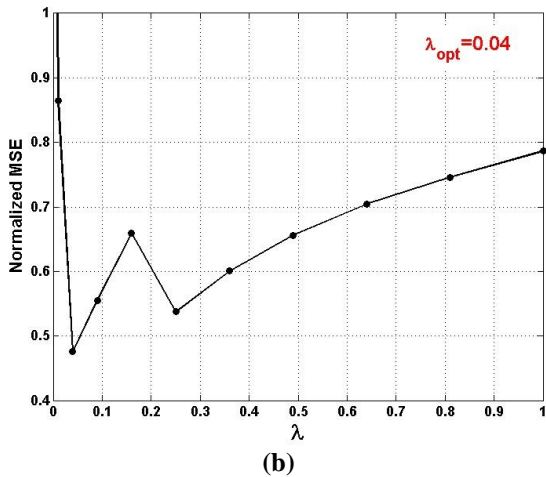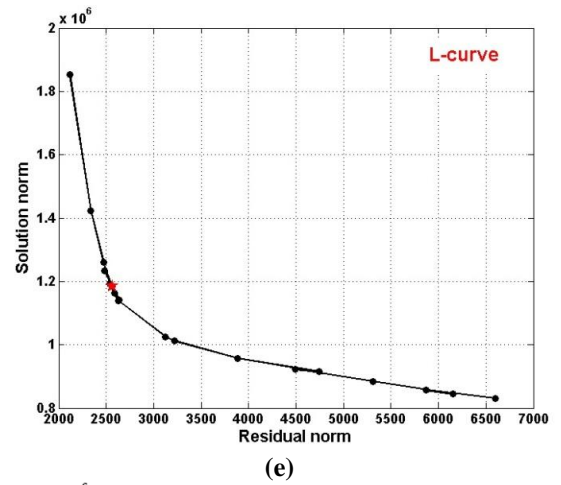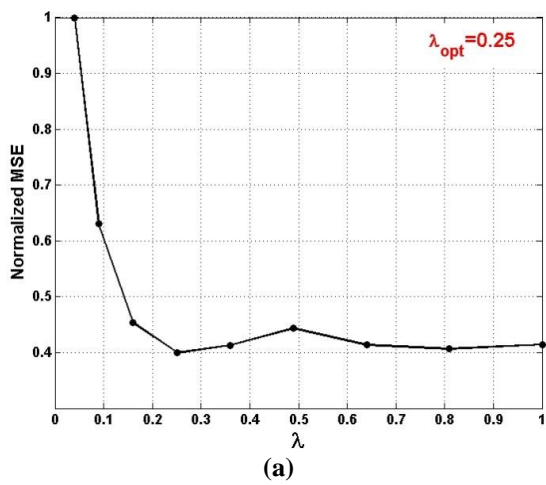

Figure 4. Regularization parameter λ selection using L-curve for four different levels. Left panel shows the normalized MSE score versus λ at which the optimum value of λ minimizes the MSE for downward continued levels of (a) 1.5 m, (b) 1 m, (c) 0.5 m, (d) 0 m. Right panel shows the L-curve for downward levels of (e) 1.5 m, (f) 1 m, (g) 0.5 m, (h) 0 m. The optimum values of the MSE scores have been superimposed on the L-curve plots with a red asterisk symbol.

(c)

(g)

(d)

(h)
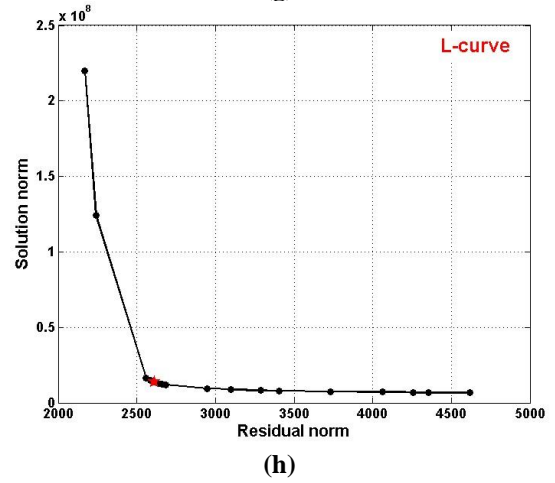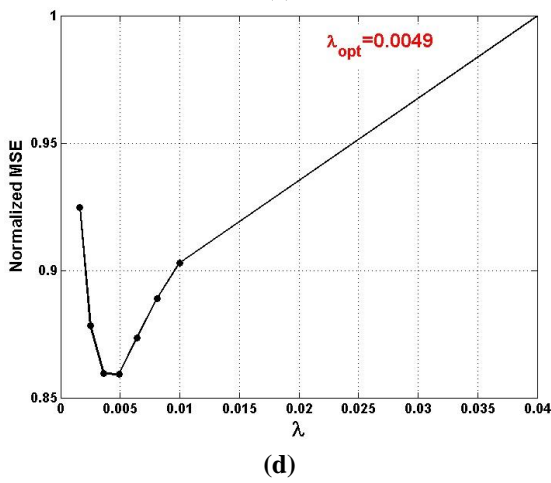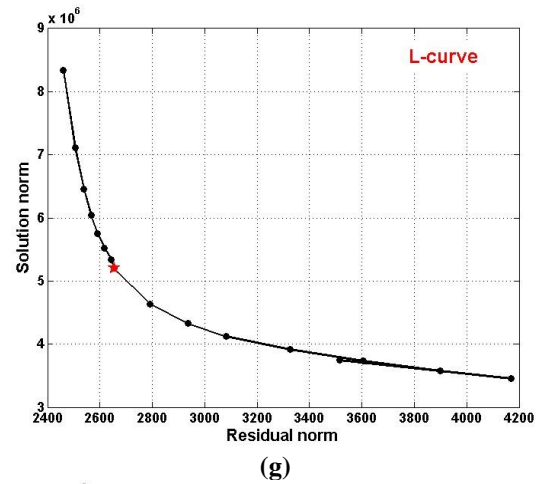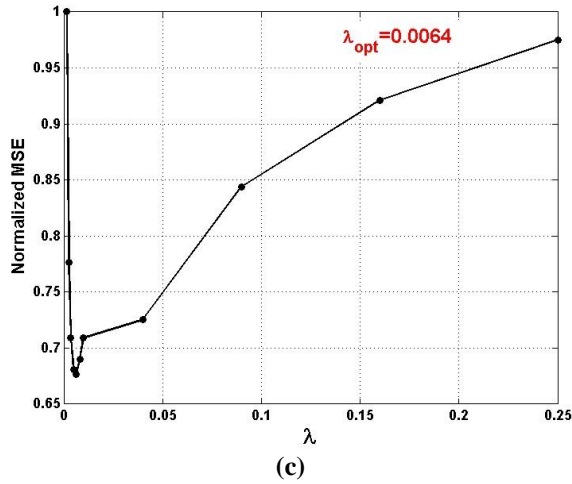
Figure 4. Continued.

4. Real case study

The real case study is a magnetic gradient survey provided by Barthel & Schriber GmbH, Cologne, Germany [55]. It forms part of a much larger dataset collected within Germany to detect UXO buried in the sediments of the Rhine River. The data were collected using a towed array of gradiometers with a sensor height of 0.55 m. The conducted survey has a sample interval along line of 0.10 m, and 0.70 m of line spacing. Figure 5a shows the magnetic gradiometry map. The total magnetic data over the study area was calculated from the gradiometry map shown in Figure 5b. To apply the edge-preserved stable downward continuation method, the optimum value of the regularization parameter was chosen equal to 900 based on the L-cure plot shown in Figure 6. This amount of the regularization parameter corresponds to a point at which the L-curve plot attains the maximum curvature, i.e. balancing the solution norm and misfit data in the cost function of inverse problem. The

aforementioned results in synthetic data modeling proved that this point is in accordance with the optimum value of the regularization parameter. Therefore, the stable downward continuation filter is applied to the original data at height of 0.55 m over the study area in order to amplify the observed magnetic signals provided that suppresses the noise effects. The 0.55-m downward continued solution is shown in Figure 7a while the signal-to-noise ratio increased. Since the amplitude of magnetic signals are strengthened, the analytic signal map of the downward solution was used as well to enhance more the locations of the probable causative UXO sources in Figure 7b. As it is obvious, these enhanced signals can correspond to UXOs that should be noted as probable sources of danger when encountering with the contaminated area. Therefore, these sources can be investigated in order to be cleaned up.

(a)

(b)
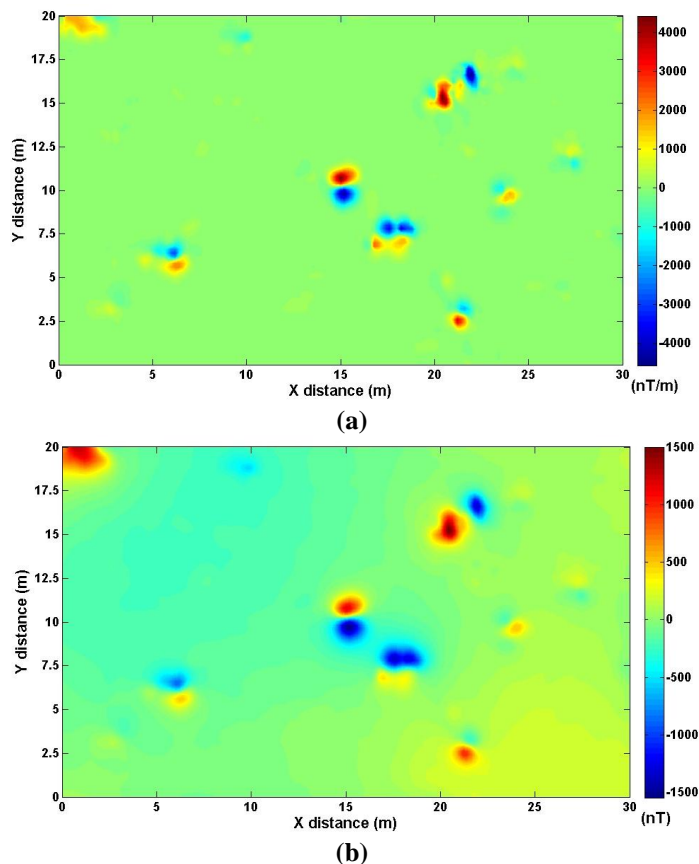
Figure 5. The real observed magnetic anomaly over the area contaminated by UXO [55], (a) the magnetic gradiometry data at height of 0.55 m, (b) the calculated total magnetic data.
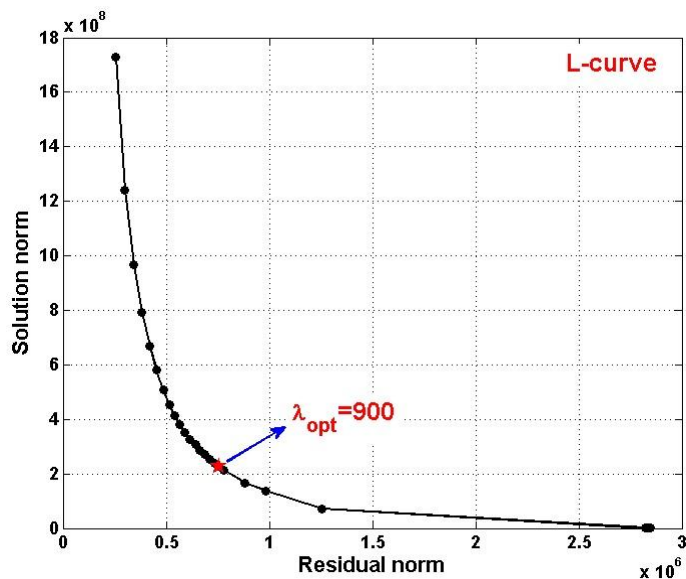

Figure 6. The L-curve plot of the real magnetic anomaly for downward continued level of 0.55 m. The optimum value of the regularization parameter λ is 900.
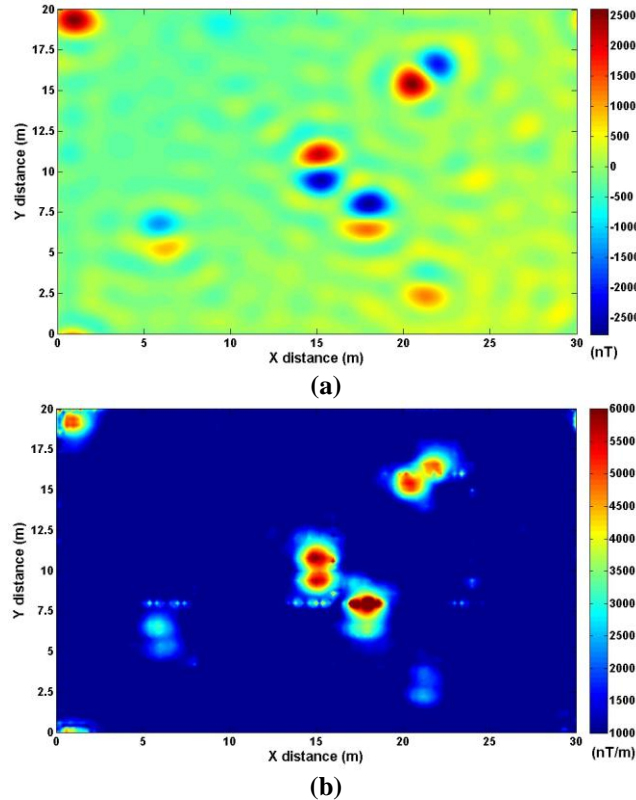
Figure 7. The stable downward continuation of the real magnetic data shown in Figure 5b, (a) the 0.55-m downward continued data, (b) the analytic signal of the downward continued data which enhances the locations of probable UXOs in the study area.

5. Conclusions

This study confirms the efficiency of a powerful method in stably downward continuation of magnetic data in UXO detection using the edge-preserved technique. It shows that getting closer to the ground surface in magnetic prospect increases the signal-to-noise ratio, which subsequently causes the location separation of the multi-source UXO in the contaminated territories. The proposed method could effectively regularize the downward solution in Fourier domain by suppressing the noise effect when continuing the data. Both synthetic and real case study data indicate the capability of the applied method to amplify the magnetic signal strength when the observed data continue to the ground surface. As a result in magnetic prospect of UXO sources, amplification of the observed signals by applying the stable downward continued approach can appropriately separate the locations of probable causative sources, especially when small UXOs exist at the contaminated territories.

References

[1]. Pawlowski, J. (1994). Ordnance Investigation Using an Electromagnetic Method, Lake Erie, Port Clinton, Ohio, report for USAE Waterways Experiment Station, by Geophysics Ltd., Mississauga, Ontario.

[2]. Pawlowski, J., Lewis, R., Dobush, T. and Valleau, N. (1995). Proceeding of the Symposium on the Application of Geophysics to Engineering and Environmental Problems, Orlando, Florida, USA.

[3]. Butler, D.K. (2000). Assessment of Microgravity for UXO Detection and Discrimination. U.S. Army Engineer Research and Development Center: 1-37.

[4]. Butler, D.K. (2003). Implications of magnetic backgrounds for unexploded ordnance detection. Journal of Applied Geophysics, 54: 111-125.

[5]. Bell, T., Barrow, B., Miller, J. and Keiswetter, D. (2001). Time and Frequency Domain Electromagnetic Induction Signatures of Unexploded Ordnance. Subsurface Sensing Technology and Applications, 2: 153-175.

[6]. Beard, L.P., Doll, W.E., Holladay, J.S., Gamey, T.J., Lee, J.L.C. and Bell, D.T. (2004). Field tests of an experimental helicopter time-domain electromagnetic system for unexploded ordnance detection. Geophysics, 69: 664-673.

[7]. Pasion, L.R., Billings, S.D., Oldenburg, D.W. and Walker, S.E. (2007). Application of a library based method to time domain electromagnetic data for the identification of unexploded ordnance. Journal of Applied Geophysics, 61: 279-291.

[8]. Sanchez, V., Li, Y., Nabighian, M.N. and Wright, D.L. (2008). Numerical Modeling of Higher Order Magnetic Moments in UXO Discrimination. IEEE Trans. Geosci. Remote Sens., 46: 2568-2583.

[9]. Davis, K., Li, Y. and Nabighian, M.N. (2010). Automatic detection of UXO magnetic anomalies using extended Euler deconvolution. Geophysics, 75: G13-G20.

[10]. Davis, K., Li, Y. and Nabighian, M.N. (2011). Effects of low-pass filtering on the calculated structure index from magnetic data. Geophysics, 76: L23-L28.

[11]. Li, Y., Devriese, S.G.R., Krahenbuhl, R. and Davis, K. (2013). Enhancement of Magnetic Data by Stable Downward Continuation for UXO Application. IEEE Trans. Geosci. Remote Sens., 51: 3605-3614.

[12]. Pederson, A. and Stalcup, B. (1997). Phase III advanced technology demonstrations at Jefferson proving ground. Proceedings of the UXO Forum' 97: pp. 281 – 289.

[13]. Bruschini, C., Gros, B., Guerne, F., Piéce, P.Y. and Carmona, O. (1998). Ground penetrating radar and imaging metal detector for antipersonnel mine detection. Journal of Applied Geophysics, 40: 59-71.

[14]. Huang, H. and Won, I.J. (2000). Conductivity and Susceptibility Mapping Using Broadband Electromagnetic Sensors. Journal of Environmental and Engineering Geophysics, 5: 31-41.

[15]. Koppenjan, S.K., Allen, C.M., Gardner, D., Wong, H.R., Lee, H. and Lockwood, S.J. (2000). Multi-frequency synthetic-aperture imaging with a lightweight ground penetrating radar system. Journal of Applied Geophysics, 43: 251-258.

[16]. Butler, D.K. (2001). Potential fields methods for location of unexploded ordnance. The Leading Edge, 20: 890 – 895.

[17]. Butler, D.K., Wolfe, P.J. and Hansen, R.O. (2001). Analytical modeling of magnetic and gravity signatures of unexploded ordnance. Journal of Environmental and Engineering Geophysics, 6: 33 – 46.

[18]. Huang, H. and Won, I.J. (2003). Characterization of UXO-Like Targets Using Broadband Electromagnetic Induction Sensors. IEEE Trans. Geosci. Remote Sens., 41: 652-663.

[19]. Huang, H. and Won, I.J. (2003). Detecting metal objects in magnetic environments using a broadband electromagnetic method. Geophysics, 68: 1877-1887.

[20]. Huang, H. and Won, I.J. (2003). Automatic anomaly picking from broadband electromagnetic data in an unexploded ordnance (UXO) survey. Geophysics, 68: 1870-1876.

[21]. Huang, H. and Won, I.J. (2004). Electromagnetic detection of buried metallic objects using quad-quad conductivity. Geophysics, 69: 1387-1393.

[22]. Benavides, A. and Everett, M.E. (2007). Non-linear inversion of controlled source multi-receiver electromagnetic induction data for unexploded ordnance using a continuation method. Journal of Applied Geophysics, 61: 243-253.

[23]. Billings, S.D. and Youmans, C. (2007). Experiences with unexploded ordnance discrimination using magnetometry at a live-site in Montana. Journal of Applied Geophysics, 61: 194-205.

[24]. Huang, H., SanFilipo, B., Oren, A. and Won, I.J. (2007). Coaxial coil towed EMI sensor array for UXO detection and characterization. Journal of Applied Geophysics, 61: 217-226.

[25]. Billings, S.D. and Wright, D. (2010). Interpretation of high-resolution low-altitude helicopter magnetometer surveys over sites contaminated with unexploded ordnance. Journal of Applied Geophysics, 72: 225-231.

[26]. Butler, D.K., Simms, J.E., Furey, J.S. and Bennett, H.H. (2012). Review of Magnetic Modeling for UXO and Applications to Small Items and Close Distances. Journal of Environmental and Engineering Geophysics, 17: 53-73.

[27]. Butler, D.K., Cespedes, E.R., Cox, C.B. and Wolfe, P.J. (1998). Multisensor methods for buried unexploded ordnance detection, discrimination, and identifications, Technical Report SERDP-98-10, US Army Engineer Waterways Experiment Station, Vicksburg, MS.

[28]. Butler, D.K, Cespedes, E., O'Neill, K., Arcone, S., Llopis, J., Curtis, J., Cullinane, J. and Meyer, C. (1998). Overview of science and technology program for JPG phase IV. Proceedings of the UXO Forum '98, Anaheim, CA.

[29]. Keiswetter, D. (2000). Advances in frequency domain electromagnetic induction techniques for improved discrimination and identification of buried

unexploded ordnance. Proceedings of the UXO/Countermine Forum 2000, Anaheim, CA.

[30]. Pasion, L.R. and Oldenburg, D.W. (2001). A discrimination algorithm for UXO using time domain electromagnetics. Journal of Engineering and Environmental Geophysics, 6: 91 – 102.

[31]. Moreau, F., Gilbert, D. and Saracco G. (1996). Filtering non stationary in geophysical data with orthogonal wavelets. Geophys. Res. Lett., 23: 407-410.

[32]. Trompat, H., Boschetti, F. and Hornby, P. (2003). Improved downward continuation of potential field data. Exploration Geophysics, 34: 249-256.

[33]. Daubechies, I., Defrise, M. and De Mol, C. (2004). An iterative thresholding algorithm for linear inverse problems with a sparsity constraint. Communications on Pure & Applied Mathematics. 57: 1413–1457.

[34]. Davis, K. and Li, Y. (2011). Fast solution of geophysical inversion using adaptive mesh, space-filling curves and wavelet compression. Geophys. J. Int., 185: 157-166.

[35]. Boschetti, F., Hornby, P. and Horowitz, F. (2001). Wavelet based inversion of gravity data. Exploration Geophysics, 32: 48-55.

[36]. Cooper, G. (2004). The stable downward continuation of potential field data. Exploration Geophysics, 35: 260-265.

[37]. Xu, S., Yang, J., Yang, C., Xiao, P., Chen, S. and Guo, Z. (2007). The iteration method for downward continuation of a potential field from a horizontal plane. Geophysical Prospecting, 55: 883-889.

[38]. Pašteka, R., Karcol, R., Kušnirák, D. and Mojzeš, A. (2012). REGCONT: A Matlab based program for stable downward continuation of geophysical potential fields using Tikhonov regularization. Computers & Geosciences, 49: 278-289.

[39]. Amini, A., Fazel Bidgoli, Y. and Rokn Abadi, H.H.H. (2010). Linear filter for upward- down ward continuation by using wavelet transform and its application in magnetic data processing. Journal of The Earth And Space Physics, 36: 25-39.

[40]. Fedi, M. and Florio, G. (2002). A stable downward continuation by using ISVD method. Geophys. J. Int., 151: 146-156.

[41]. Guoqing, M. Liu, C., Huang, D. and Li, L. (2013). A stable iterative downward continuation of potential field data. Journal of Applied Geophysics, (In Press).

[42]. Jin-Sheng, N., Hai-Hong, W. and Zhi-Cai, L. (2005). Downward Continuation of Gravity Signal Based om The Multiscale Edge Constraint. Chinese Journal of Geophysics, 48: 74-80.

[43]. Ridsdill-Smith, T.A. and Dentith, M.C. (2000). Drape corrections of aeromagnetic data using wavelets. Exploration Geophysics, 31: 39-46.

[44]. Abedi, M., Gholami, A. and Norouzi, G.H. (2013). A stable downward continuation of airborne magnetic data: A case study for mineral prospectivity mapping in Central Iran. Computers & Geosciences, 52: 269-280.

[45]. Blakely, R.J. (1995). Potential theory in gravity and magnetic applications: Cambridge Univ. Press.

[46]. Aster, R.C., Borchers, B. and Thurber, C. (2003). Parameter Estimation and Inverse Problems. Academic Press, New York, NY.

[47]. Charbonnier, P., Blanc-Feraud, L., Aubert, G., Barlaud., M. (1997). Deterministic edge-reserving regularization in computed imaging. IEEETrans. Image Process., 6: 298–310.

[48]. Bertero-Aguirre, H., Cherkaev, E., Oristaglio, M. (2002). Non-smooth gravity problem with total variation penalization functional. Geophysical Journal International, 149: 499-507.

[49]. Candes, E.J., Guo, F. (2002). New multiscale transforms, minimum total variation synthesis: applications to edge-preserving image reconstruction. Signal Processing, 82: 1519-1543.

[50]. Gholami, A., Siahkoohi, H.R. (2009). Simultaneous constraining of model and data smoothness for regularization of geophysical inverse problems. Geophysical Journal International, 176: 151–163.

[51]. Caratori Tontini, F., Cocchi, L. and Carmisciano, C. (2006). Depth-to-the-bottom optimization for magnetic data inversion: Magnetic structure of the Latium volcanic region, Italy. Journal of Geophysical Research, 111: 1-17.

[52]. Hansen, P. and O'Leary, D. (1993). The use of the L-curve in the regularization of discrete ill-posed problems. SIAM J. Scient. Comput., 14: 1487–1503.

[53]. Lide, D.R. (2001). CRC Handbook of Chemistry and Physics. 82nd ed. Boca Raton, FL: CRC Press.

[54]. Billings, S.D, Pasion, C., Walker, S. and Beran, L. (2006). Magnetic models of unexploded ordnance. IEEE Trans. Geosci. Remote Sens., 44: 2115-2124.

[55]. Whitehead, N. (2007). Montaj UX-Detect^{TM}, Tutorial and User Guide. 105 P.